Acta Crystallographica Section B
Structural Science
ISSN 0108-7681

Tilt and acoustic instabilities in ABX_4, A_2BX_4 and ABX_3 perovskite structure types: their role in the incommensurate phases of the organic–inorganic perovskites

Ian Peter Swainson

Canadian Neutron Beam Centre, National Research Council of Canada, Chalk River Laboratories, Chalk River, Ontario, Canada K0J 1J0

Correspondence e-mail: ian.swainson@nrc.gc.ca

Received 17 March 2005
Accepted 12 September 2005

An examination of the tilt modes and other low-frequency modes is made for an isolated, untilted perovskite layer, which maps very simply to the ABX_4 perovskites. A sheet of pure tilts exists at the Brillouin Zone boundary at $\{\xi, \frac{1}{2}, \zeta\}$. An instability is also found at all wavevectors which can be described as continuously varying from pure tilts to pure layer displacements as a function of the wavevector. Analysis is extended by considering the stacking of layers in the I-centered A_2BX_4-layer perovskites. The effect of freezing in the commensurate tilt required to generate the *Cmca* tilt system, pertinent to the modulated phases of propylammonium salts, is examined. The zero-frequency modes are restricted to two planes in the Brillouin Zone. All of the observed wavevectors associated with modulated phases, and the commensurately tilted propylammonium tetrachlorocadmate, are consistent with this calculation. The effect of full three-dimensional connectivity is briefly reviewed for the true ABX_3 perovskites. While pure tilt incommensurates appear to be hypothetically possible, they do not appear to have been observed to date.

1. Introduction

True perovskites are fully corner-bonded framework structures. They are usually represented by the formula ABX_3, in which A is a cation sitting in the interstices between fully corner-bonded $BX_{6/2}$ octahedral anions. A recent overview of perovskites and related forms has been given by Mitchell (2002). There is a set of phase transitions called the tilt transitions, whose driving force can be understood as being instabilities against rotations of octahedra. There are a finite number of periodic tilt systems. Glazer (1972, 1975) first classified these tilts in direct space and developed a notation scheme for them. The commensurate tilt transitions have also been the study of a number of group-theory analyses, examining high-symmetry points of the Brillouin Zone (BZ) for representations that transform as pure rotations, that necessarily retain undistorted octahedra. Most recently this has been done by Howard & Stokes (1998, 2002), who limited the number of tilt transitions to 15. Aleksandrov *et al.* (1987) also performed analyses based on group theory, performed a major review of tilt systems, and developed an alternative notation for tilt systems. All tilt transitions are caused by modes that do not require distortion of the octahedra, although distortion may occur due to coupling to secondary-order parameters.

Hua (1991) performed a symmetry and phonon eigenvector study of the true perovskite $CsPbCl_3$, examining it for tilt modes of rigid octahedra. In addition, Giddy *et al.* (1993) presented the results for the true perovskites using one of the first applications of a phonon method developed by Dove and

coworkers (Dove *et al.*, 1991; Hammonds & Dove, 1994) for examining displacive transitions in framework structures. This method also assumes that the octahedra are perfectly rigid. In addition it makes the mathematical approximation that each octahedron has all six corner atoms. The shared corners are then re-imposed mathematically by exactly overlapping the corner atoms and putting a strong force constant before them: the split-atom method. Modes whose eigenvectors do not require distortion of the octahedral connectivity have zero frequency and are generally termed Rigid Unit Modes (RUMs). These have finite but low frequency in real crystals, but provide low-lying candidate soft modes for the crumpling of frameworks (Dove *et al.*, 1991; Giddy *et al.*, 1993; Hammonds & Dove, 1994). The rotational RUMs in a perovskite are more traditionally referred to as tilt modes.

In addition to the true perovskites there are a number of related structure types. The most closely related are the layer or sheet perovskites (Fig. 1). These can form if there is insufficient space to accommodate a given A cation in a three-dimensional framework. Rather than remaining in an enclosed cavity, the network structure can be envisioned as being pulled apart into layers and the cation placed between them, leaving unconcatenated apical atoms of the octahedra sticking out from the layers. Layer structures exist with the general formula ABX_4 with a maximum symmetry of $P4/mmm$, and A_2BX_4 with a maximum symmetry of $I4/mmm$. Several group theory and phonon eigenvector studies have been performed on these layer perovskites (Hatch & Stokes, 1985, 1987, 1989; Deblieck *et al.*, 1985; Deblieck, 1986; Bulou *et al.*, 1983, 1984, 1987; Aleksandrov *et al.*, 1987).

A rigid isolated polyhedron, such as a propylammonium cation (Doudin & Heine, 1990), has 6 degrees of freedom: three translations and three rotations. Once polyhedra are concatenated, such as is the case for the octahedral anions in a perovskite layer, the corner bonding acts as a constraint. If two polyhedra possess a common corner, this imposes three constraints in the form of the positional coordinates x, y and z of the corner atom, so that 1.5 constraints are generated per corner per polyhedron. Therefore, it is the inorganic anions of the organic–inorganic layer perovskites that restrict the flexibility of the system, as they are more intrinsically constrained than the organic cations.

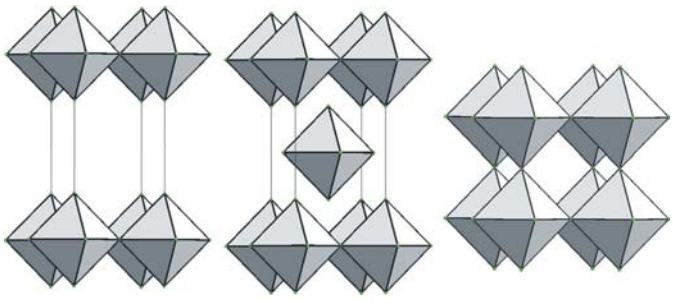

Figure 1
Aristotypes of the ABX_4 layer perovskite with symmetry $P4/mmm$ (left), A_2BX_4 (middle) with symmetry $I4/mmm$, and true perovskites (right) with symmetry $Pm3m$. The A cations are omitted.

Framework structures consisting of octahedra are generally a good deal less flexible than their tetrahedral counterparts (Hammonds, Bosenick, Dove & Heine, 1998); the number of constraints for an ABX_3 perovskite is $(6 \times 3/2) = 9$ and for layer perovskites the number of constraints is $(4 \times 3/2) = 6$. Therefore, true perovskites are overconstrained and only a small number of excess modes exist even in the highest symmetry phase (Giddy *et al.*, 1993; Hammonds, Bosenick, Dove & Heine, 1998). However, from this simple counting a layer of corner-bonded octahedra is exactly constrained and would not be expected to be any floppier than a three-dimensional framework built of tetrahedra, which is also exactly constrained. The role of symmetry is highly important since high symmetry makes some of these constraints degenerate and not independent (Dove *et al.*, 1991; Giddy *et al.*, 1993; Hammonds & Dove, 1994) and it is only for this reason that the sparse set of tilt modes exists along the high-symmetry direction M–T–R in the overconstrained ABX_3 perovskites (Giddy *et al.*, 1993). Once tilting has occurred and symmetry is reduced it is to be expected that the number of such zero-frequency modes will decrease (Dove *et al.*, 1991; Giddy *et al.*, 1993; Hammonds & Dove, 1994).

1.1. Organic–inorganic perovskites

There is a class of perovskites in which the A cation is replaced by a molecular cation, usually an amine or diamine. Methylammonium (MA), formamidinium (FA) and tetramethylammonium (TMA) have all been reported as occurring in true perovskite structures (*e.g.* Depmeier, 1981; Poglitsch & Weber, 1987; Mitzi & Liang, 1997; Lee *et al.*, 2003; Swainson *et al.*, 2003; Chi *et al.*, 2005). Organic chains can essentially be arbitrarily long, so the majority of organic–inorganic perovskites crystallize in a layer perovskite form, as only the smallest chained amines can fit inside the three-dimensional framework structure of the true perovskites. There is, therefore, a great structural variety of these forms and many show interesting electrical properties (Mitzi, 2001). This class of perovskites has become known as the organic–inorganic perovskites.

The short-chained amine cations can be quite rigid. Even for chains such as propylammonium (PA), whose salts crystallize as layer perovskites, the cation can be viewed as relatively rigid (Doudin & Heine, 1990). It is only as the chain length increases that the organic cations possess a high degree of flexibility (*e.g.* Barman *et al.*, 2003). For the methylammonium lead halides, Rietveld refinements and crystal chemical trends have shown that the molecular cations are more rigid than the octahedra; it is the octahedra, approximated as rigid units in both the RUM and group theory approaches to tilt transitions (Glazer, 1972, 1975; Bulou *et al.*, 1983, 1984, 1987; Deblieck *et al.*, 1985; Deblieck, 1986; Hatch & Stokes, 1985, 1987, 1989; Aleksandrov *et al.*, 1987; Hua, 1991; Dove *et al.*, 1991; Giddy *et al.*, 1993; Hammonds & Dove, 1994; Howard & Stokes, 1998, 2002), that distort in preference to the molecular cations in the low-temperature phases (Swainson *et al.*, 2003; Chi *et al.*, 2005). This observation in the ordered structures

agrees with the dynamics measured by Raman spectra, which show that even the lowest-frequency Raman-active internal mode of the MA cation is higher than the highest-frequency internal mode of the $PbCl_6$ octahedra of $MAPbCl_3$ (Maalej *et al.*, 1997, 1999). Despite this, the ordered phases are related to the tilt modes, with symmetries sometimes slightly lower than those predicted for perovskites with simple cations, owing in part to superlattice formation as the cations order (Chi *et al.*, 2005); these are systems in which the tilt transitions, intrinsic to the connectivity of the inorganic layer, are coupled to orientational-ordering transitions, which are intrinsic to the organic cations.

1.2. Incommensurates

An examination of the true perovskites reveals several reported to date with incommensurate structures, *e.g.* $MAPbCl_3$ and $TMAGeCl_3$ (Depmeier, 1981; Fütterer *et al.*, 1995; Kawamura & Mashiyama, 1999). Kawamura & Mashiyama (1999) reported a 'superstructure' for an intermediate phase of $MAPbBr_3$. The structure of $TMAGeCl_3$ has been very well characterized (Depmeier, 1981; Fütterer *et al.*, 1995). The incommensurate phases do not appear in analogous inorganic perovskites with simple cations. In the incommensurate structures commonly reported in layer perovskites with the *n*-propylammonium cation, modulations appear at a variety of wavevectors. In several cases more than one incommensurate phase occurs on cooling (Muralt, 1986; Kind & Muralt, 1986; Muralt *et al.*, 1988).

Incommensurate structures consist of a regular three-dimensional lattice upon which a distortional wave has been superimposed and where the ratio of the wavelength to that of the unit-cell dimensions is not a rational number. In three dimensions the structure is therefore aperiodic, although these structures may be viewed as being periodic in higher dimensions (de Wolff *et al.*, 1981). One mode of generation of incommensurates is due to the instability at the electronic Fermi surface. As organic–inorganic perovskites can show a variety of electronic transitions (Mitzi, 2001) this seems a possible mode of origin, but it does not explain the prevalence across many different metals in the same series, *e.g.* the *n*-propylammonium salts show incommensurate phases with many metal cations (Chapuis, 1978; Muralt, 1986; Kind & Muralt, 1986; Etxebarria *et al.*, 1988; Doudin & Chapuis, 1988). Another mechanism for incommensurate transitions, not related to electronic instabilities, is the condensation of soft phonons at a position other than a zone centre or boundary position of the BZ. Phonons with intrinsically low frequencies are ideal candidates for involvement in these transitions. These candidates include tilt and general acoustic modes.

The general picture of incommensurate phases includes competition between two interactions or between two ordering processes, both of which transform as the same symmetry (Levanyuk, 1986). The model of Heine & McConnell (1981) may provide a general explanation for the incommensurate transitions in both layered and true perovskites. In this model a low-lying branch, which may be an acoustic mode, interacts with a descending low-frequency optic mode. The symmetries of these two modes are different at the zone centre and boundary, but identical at all intermediate wavevectors. An anti-crossing interaction mutually repels these two phonon branches, causing the softening at non-high symmetry points of the BZ and incommensurate transition. The resulting distortion may be of mixed character in terms of the eigenvectors of the two modes. This model gives a very general description of the transition, but a microscopic basis can be gained if one considers the possible low-frequency modes that may be involved. In addition, the symmetry constraints for interaction can provide information which is useful in interpretating the transition.

Doudin & Heine (1990) proposed a microscopic model for PA tetrachlorometallates that concentrated on the interactions between the PA chains. This suggested that the PA chains provide the driving force for incommensuration in this compound, a view that has support from NMR studies (Kind & Muralt, 1986). The pitch of the alkyl chains is determined by the conformation of the octahedral layer to which the chains start to hydrogen bond *via* their amine groups on cooling. This chain spacing is not at a minimum in energy (Doudin & Heine, 1990). Moving the chains closer or further apart, which can be achieved by an incommensurate modulation of the chains, can lower the energy of the system. This is achieved by coupling to the buckling of the layers, in such a way that neighbouring layers are out of phase. However, no detailed examination of the response of the layers appears to have been made previously.

This work was started in order to see whether the RUM approach, which has proved to be very successful in the analysis of framework structures, could shed some light on the origin of the number of incommensurate phases reported in PA salts and the flexibility of the wavevectors. A search of various types of low-frequency modes intrinsic to the various perovskite structure types is made to find candidates for participation in incommensurate transitions. The treatment of the incommensurate structures of A_2BX_4 has historically concentrated on the interactions between the rigid amine chains (Muralt, 1986; Kind & Muralt, 1986; Muralt *et al.*, 1988; Doudin & Heine, 1990) and has not explicitly treated the response of the perovskite layer. As the interactions between the organic chains are transmitted to the inorganic layers *via* hydrogen bonds, there is an implicit assumption that the perovskite layers are flexible at arbitrary **k**.

In the following, the opposite approach is taken; the amine cations are ignored and the low-frequency modes of perovskite layers are examined. It is shown that an untilted layer is indeed flexible at all points in the BZ. However, *Cmca* commensurately tilted layers, from which the modulated phases descend, show a distinct anisotropy in the form of two soft planes.

2. Methods

The split-atom lattice dynamics code CRUSH of Hammonds & Dove (1994) was used to analyze the zero-frequency modes

as a function of wavevector. Ideal octahedra were used in every case. The eigenvectors of the split-atom phonon spectrum were compared with those given from the group analysis program *ISOTROPY* (Stokes & Hatch, 2002). At any given point in the BZ the irreducible representations were examined to see how the basis vectors transform for the centres of the octahedra (*e.g.* as rotations and translations), using the approach of Howard & Stokes (1998). Compatibility relations were also calculated using this program. The labelling used for the mode symmetry is that of Miller & Love (1967), except at the zone centre where Mulliken labels for the representations are also given. Owing to the ease of illustration the method will be first applied to the ABX_4 perovskites and then to the A_2BX_4 and ABX_3 perovskites.

3. Intrinsic instabilities for isolated perovskite layers in a primitive tetragonal lattice

A single perovskite layer of ideal octahedra was modelled using *CRUSH* (Hammonds & Dove, 1994). When placed in a three-dimensional lattice, the simplest way of packing these layers is in a primitive tetragonal lattice, whose maximum symmetry is *P*4/*mmm*. This model therefore directly maps to the ABX_4-layer perovskites, which have this symmetry in their untilted (aristotype) form. The BZ of the primitive tetragonal lattice is shown in Fig. 2.

In any structure there is always one set of zero-frequency solutions, which are the Γ-point acoustic modes, for which all atoms move in-phase. In this hypothetical model there is no interaction between layers stacked along **c**. This results in the acoustic modes having zero-frequency along Γ–Λ–*Z* (Table 1, Fig. 2). These represent the longitudinal and transverse translations of whole layers: T_z and (T_x, T_y), against which there is no restoring force. Clearly, as soon as any coupling is introduced these would gain a finite frequency away from the Γ point. Bulou *et al.* (1983, 1984, 1987) have shown that once coupling is introduced the acoustic dispersion in ABX_4 perovskites along this direction remains small.

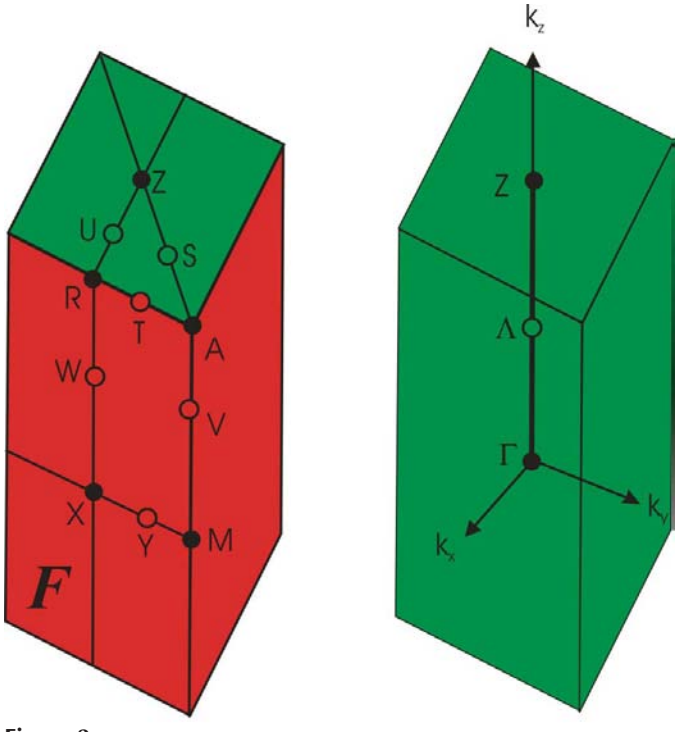

Figure 2
Brillouin Zone (BZ) of the primitive tetragonal lattice. Left: The outer surface of the BZ with high symmetry points (closed) and directions (open) shown as circles. The surface F on which a general plane of tilts occurs is shaded red. Right: The lines of pure displacements of the Γ–Λ–*Z* layers. Buckling instabilities exist at all intermediate wavevectors.

Table 1
Points, lines and planes of zero-frequency modes in the BZ of an ideal ABX_4 perovskite with *P*4/*mmm* symmetry.

The nature of the eigenvectors of selected zero-frequency modes are given, where *T* represents the translation along an axis and *R* the rotation about an axis. Those labeled 'mixed' have complex eigenvectors with components of T_z and (R_x, R_y) and represent buckling instabilities.

	k	Nature	Symmetry	Nature	Symmetry
Γ	{0,0,0}	T_z	Γ_3^- A_{2u}	(T_x, T_y)	Γ_5^- E_u
Λ	{0,0,ξ}	T_z	Λ_1	(T_x, T_y)	Λ_5
Z	{0,0,$\frac{1}{2}$}	T_z	Z_3^-	(T_x, T_y)	Z_5^-
M	{$\frac{1}{2}$,$\frac{1}{2}$,0}	(R_x, R_y)	M_5^+	R_z	M_3^+
V	{$\frac{1}{2}$,$\frac{1}{2}$,ζ}	(R_x, R_y)	V_5	R_z	V_4
A	{$\frac{1}{2}$,$\frac{1}{2}$,$\frac{1}{2}$}	(R_x, R_y)	A_5^+	R_z	A_3^+
X	{0,$\frac{1}{2}$,0}	(R_x, R_y)	X_3^+		
W	{0,$\frac{1}{2}$,ξ}	(R_x, R_y)	W_3		
R	{0,$\frac{1}{2}$,$\frac{1}{2}$}	(R_x, R_y)	R_3^+		
Y	{ξ,$\frac{1}{2}$,0}	(R_x, R_y)	Y_2		
F	{ξ,$\frac{1}{2}$,ζ}	(R_x, R_y)	F_2		
T	{$\frac{1}{2}$,ξ,$\frac{1}{2}$}	(R_x, R_y)	T_2		
S	{ξ,ξ,$\frac{1}{2}$}	Mixed	S_3		
U	{0,ξ,$\frac{1}{2}$}	Mixed	U_3		
Δ	{0,ξ,0}	Mixed	Δ_3		
Σ	{ξ,ξ,0}	Mixed	Σ_3		

The CRUSH calculations along the zone-boundary *M*–*V*–*A* show zero-frequency modes. These have the characteristics of pure rotations (tilt modes) around the three crystal axes, R_x, R_y and R_z. Hua (1989) showed that the symmetry of the vibration modes along *M*–*V*–*A* are 'essentially the same'. Similarly, pure tilts are found at the high-symmetry points *X* and *R*, and along the *W* line linking them (Fig. 2, Table 1). Deblieck *et al.* (1985) and Deblieck (1986) examined the irreducible representations that correspond to the commensurate tilt modes at points of high symmetry in the BZ. The results of their analyses were given in terms of the convention of Bradley & Cracknell (1972), so that the labelling of the irreducible representations differs from those presented in Table 1, but the results are otherwise identical. These tilts at the *M*, *A*, *X* and *R* high-symmetry points represent special points on sheets of pure tilts, of symmetry F_2, with wavevectors {ξ, $\frac{1}{2}$, ζ} (Fig. 2, Table 1).

The CRUSH calculations also showed one zero-frequency mode for all wavevectors in the interior of the BZ. As the calculation is followed into the interior of the BZ from the F_2

sheet of pure tilts, it is found that these modes are transverse acoustic (TA) modes for which the layer is modulated with displacements along **c**. An instability at every **k** is not unknown even in three-dimensional framework structures and has been reported in some zeolites (Hammonds, Heine & Dove, 1998). The highest-symmetry silica framework, β-cristobalite, shows general planes of RUMs (Giddy *et al.*, 1993; Swainson & Dove, 1993).

The projection of an isolated perovskite layer viewed down **b** is shown in Fig. 3. When $|\mathbf{k}| = a^*/2$, $\lambda = 2a$, the centres of the octahedra sit on nodes of this transverse acoustic wave and remain in the plane of the perovskite layer so that the displacement eigenvectors become pure tilts of the octahedra (R_x, R_y). However, as λ increases and $|\mathbf{k}| \Rightarrow 0$, the octahedra, which must remain rigid and retain their interconnectivity with their neighbours, take an increasing component of displacement along the layer normal, c, giving potential buckling instabilities. In untilted ABX_4 crystals this corresponds to the compatibilities listed in Table 1, showing that the F_2 tilts become pure z-translations of entire perovskite layers for $\mathbf{k} = (0,0,\xi)$, *i.e.* the $\Gamma_3^- - \Lambda_1 - Z_3^-$ acoustic modes (Table 1, Figs. 2 and 3). The nature of these modes at arbitrary **k** is therefore rather different from the RUMs in a three-dimensional framework in which such buckling modes are not available.

There is an additional line of tilt modes, $M_3^+ - V_4 - A_3^+$, having the pseudovectors of rotation R_z parallel to the trace of the line M–V–A. These modes are not compatible with the class of buckling modes, but are a separate class of tilts in the layer perovskites. CRUSH calculations across the BZ show that M_3^+ is also a zone-boundary transverse acoustic mode, but has finite frequencies at all intermediate wavevectors and which forms one component of the Γ_5^- (T_x, T_y) mode at the zone centre.

Schematics of the eigenvectors of the pure tilt modes at high symmetry points of the BZ boundary for ABX_4 perovskites are shown in Figs. 4–6. The eigenvectors of the X_3^+–W_3–R_3^+ tilt modes given by *ISOTROPY* (Fig. 4*a*) show contributions from the star of vectors, whereas by studying individual **k** points in CRUSH one sees contributions from individual branches; observing pure R_y tilts at ($\frac{1}{2}$, 0, 0) and pure R_x tilts at (0, $\frac{1}{2}$, 0) (Fig. 4*c*).

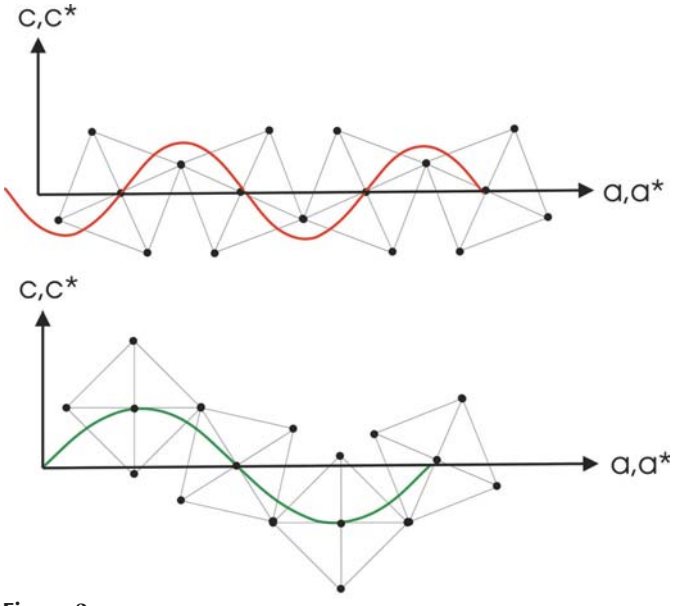

Figure 3
Illustration of the buckling instability in an isolated perovskite layer. The layer is shown edge-on viewed down the *b* axis. A transverse acoustic wave with displacements along **c** is shown with the wavevector parallel to a^*. For the special case where $\mathbf{k} = \mathbf{a}^*/2$, $\lambda = 2a$, the centres of mass sit on nodes and the modes are pure R_y tilts (top). For the general case where $\mathbf{k} < \boldsymbol{a}^*/2$, $\lambda > 2a$, the centres of mass of the octahedra are displaced, while the octahedra rotate to maintain the connectivity, thus buckling the layer (bottom).

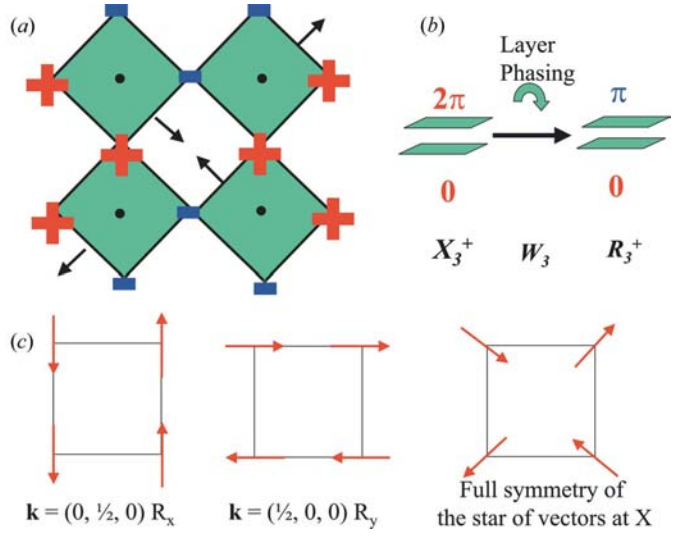

Figure 4
Eigenvectors of the X_3^+ and R_3^+ pure tilt phonons. (*a*) The pseudovectors represent the directions of clockwise rotation in an isolated layer of 2 × 2 octahedra. Vertical displacements of the shared corner atoms are shown by + and − symbols. (*b*) The relative phasing of neighbouring layers in a P-tetragonal lattice: X_3^+ transforms as layers with eigenvectors in-phase, R_3^+ out-of-phase and W_3 as continuous intermediate phasings. (*c*) The eigenvectors associated with a single arm of the X_3^+ tilt phonon at (0, $\frac{1}{2}$, 0) (left),($\frac{1}{2}$,0,0) (middle) and the star of vectors (right).

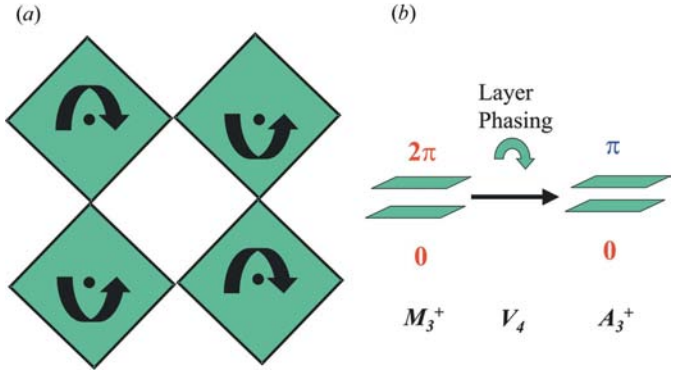

Figure 5
Eigenvectors of the M_3^+ and A_3^+ pure tilt phonons. (*a*) The directions of rotation about the *c* axis, R_z, in an isolated layer of 2 × 2 octahedra are shown. (*b*) The relative phasing of neighbouring layers in a P-tetragonal lattice: M_3^+ transforms as layers with eigenvectors in-phase, A_3^+ out-of-phase and V_4 as continuous intermediate phasings.

3.1. A direct space picture of the origin of a sheet of pure tilts

To demonstrate the freedom of phasing of tilts that exists between neighbouring perovskite layers, a projection of an isolated layer displaying the rotational eigenvectors is shown, along with a schematic of the relative phasing of the tilts between the two layers stacked along **c**. It is clear that the phasing of tilts, R_x, R_y and R_z, between isolated layers can be random with no energy penalty. Hence, the pure tilts at M and A are linked by the V line of tilts along c^*, and the pure tilts at X and R are linked along W (Fig. 2, Table 1).

The degree to which the freedom of tilt phasing exists within a single layer is not immediately obvious. A schematic of the freedom of phasing of R_y tilts is shown in Fig. 7. Owing to the relatively few constraints in a two-dimensional net, a choice of $+R_y$ for one octahedron only ensures that the octahedra in the x-column at $\pm a$ have $-R_y$. Octahedra linked at $\pm b$ have no automatically imposed sense of R_y. Therefore, complete freedom of phasing of R_y tilts exists between neighbouring x columns. This corresponds to the line of tilts joining X_3^+ and M_5^+ with symmetry Y_2, and the line R_3^+–T_2–A_5^+.

The existence of anti-correlated R_y tilts running along columns in x, with the complete freedom of phasing of R_y tilts in neighbouring columns within the same perovskite layer and between individual layers stacked on c, is the origin of the sheets of R_y tilts at $\mathbf{k} = (\pm\frac{1}{2}, \xi, \zeta)$. The degenerate R_x tilts occur in F_2 sheets $(\xi, \pm\frac{1}{2}, \zeta)$.

4. Relationship of the tilt systems of the ABX_4 layer perovskites to those of A_2BX_4 layer perovskites

Another way of stacking isolated perovskite layers is to do so by relating one layer to the next by an I-centre. This is characteristic of the A_2BX_4 layer perovskites. One can generate this by sliding alternate layers of the ABX_4 structure along $[\frac{1}{2}, \frac{1}{2}, 0]$. From the point of view of the fundamental instabilities of the layers, as the approximation is made that each layer is independent, there is no real significance to how they are stacked; the plane of pure tilt instabilities still exists with $\lambda = 2a$ ($|\mathbf{k}| = a^*/2$), determined by the connectivity of octahedra within each individual layer. However, more complicated phasings of the motions of the octahedra exist between the layers. The relationship between the BZs of the ABX_4 and A_2BX_4 perovskites is shown in Fig. 8. The N–Q–P–W–X plane contains the plane of pure tilts in this BZ. There have been a number of papers concerning the group theory of A_2BX_4 layer perovskites determining the possible commensurate tilt systems (Hatch & Stokes, 1985, 1987, 1989). Hatch & Stokes (1987) gave eigenvectors for P_5, X_3^+, X_4^+ and N_1^+. The P, N and X points are intersections of the plane of tilts with high-symmetry points of the BZ boundary (Fig. 8*b*). The X–W–P lines (Fig. 8) lie along the intersection of two planes of tilts – the analogue of the M–V–A line in the ABX_4 perovskites (Fig. 2).

The eigenvectors of the pure tilts P_5–W_3–X_4^+ and P_5–W_4–X_3^+ are the analogues of the M_5^+–V_5–A_5^+ modes in the ABX_4 perovskites. Similarly the N_1^+ commensurate tilt is the analogue to the X_3^+–W_3–R_3^+ line of tilts in the ABX_4 perovskites.

The line of modes P_4–W_2–X_2^+ (Hatch & Stokes, 1989) have eigenvectors that can be represented by R_z tilts, whose rotational pseudovectors are parallel to the trace of the P–W–X line. These are the analogues of the class of modes M_3^+–V_4–A_3^+ of the ABX_4 perovskites.

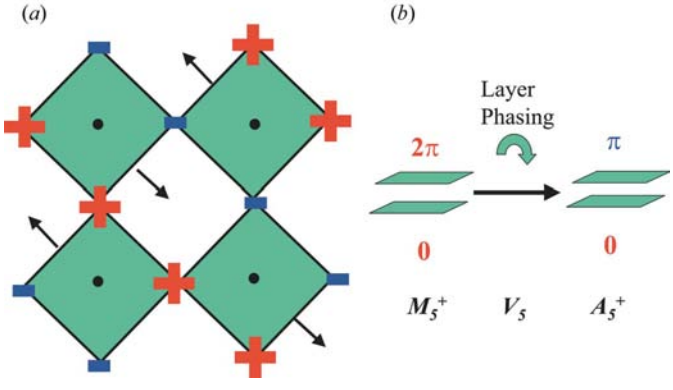

Figure 6
Eigenvectors of the M_5^+ and A_5^+ pure tilt phonons. (*a*) The pseudovectors represent directions of clockwise rotation in an isolated layer of 2 × 2 octahedra. Vertical displacements of the shared corner atoms are shown by + and − symbols. (*b*) The relative phasing of neighbouring layers in a P-tetragonal lattice: M_5^+ transforms as layers with eigenvectors in-phase, A_5^+ out-of-phase and V_5 as continuous intermediate phasings.

4.1. Incommensurate *n*-propylammonium A_2BX_4 layer perovskites

Many *n*-PA metallates show incommensurate phases on cooling. These are based around the A_2BX_4 layered perovskites with maximum symmetry $I4/mmm$. PA_2MnCl_4 shows the sequence of transitions α–β–γ–δ–ε–ζ, where α is the $I4/mmm$

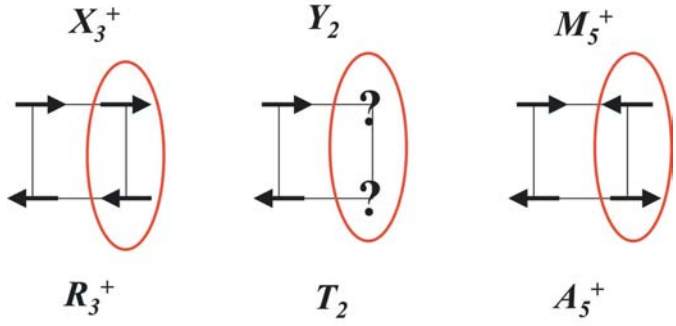

Figure 7
Origin of the sheet of R_y tilts at $a^*/2$. Eigenvectors of the acoustic phonons of X_3^+ symmetry [a single arm at $(\frac{1}{2}, 0, 0)$], M_5^+ (right), and the line joining the two, Y_2 (middle). Pseudovectors representing the axes of rotation (tilt) of the type R_y are shown. By choosing a sense of rotation of R_y on one octahedron, the only resultant action is that the octahedra along $\pm a$ has $-R_y$. There is no automatically imposed choice of R_y for octahedra connected at $\pm b$, so that a continuous variation in-phase of R_y can exist, representing the line of modes with symmetry Y_2. These same eigenvectors exist for arms of R_3^+–T_2–A_5^+ with wavevectors along the $(\frac{1}{2}, \xi, \frac{1}{2})$ line, although in this case alternate layers are out-of-phase.

maximum symmetry and β is *Cmca*, related by a pure tilt transition to α. (It should be noted that many authors have chosen the orientation of the cell for convenience to be *Abma*, to keep the layers stacked along **c**. In this paper the layers in the β phase are considered to be stacked along b in the standard *Cmca* orientation and the discussion below reflects this.) Phase δ is a re-entrant of phase β, γ and ε are incommensurate phases, and ζ is a low-temperature commensurately modulated phase (Depmeier, 1981, 1983; Depmeier & Mason, 1978). Existing theoretical treatments of the origin of the incommensurate modulations in these salts have implicitly assumed the inorganic layer is flexible at arbitrary **k**. As shown above, this assumption is valid for the untilted sheet. However, as a reduction in symmetry happens once a commensurate tilt occurs (Dove *et al.*, 1991; Giddy *et al.*, 1993; Hammonds & Dove, 1994), it is reasonable to examine the degree of flexibility after tilting, as the incommensurate phases do not descend directly from the untilted *I*4/*mmm* structure, but from the tilted *Cmca* structure.

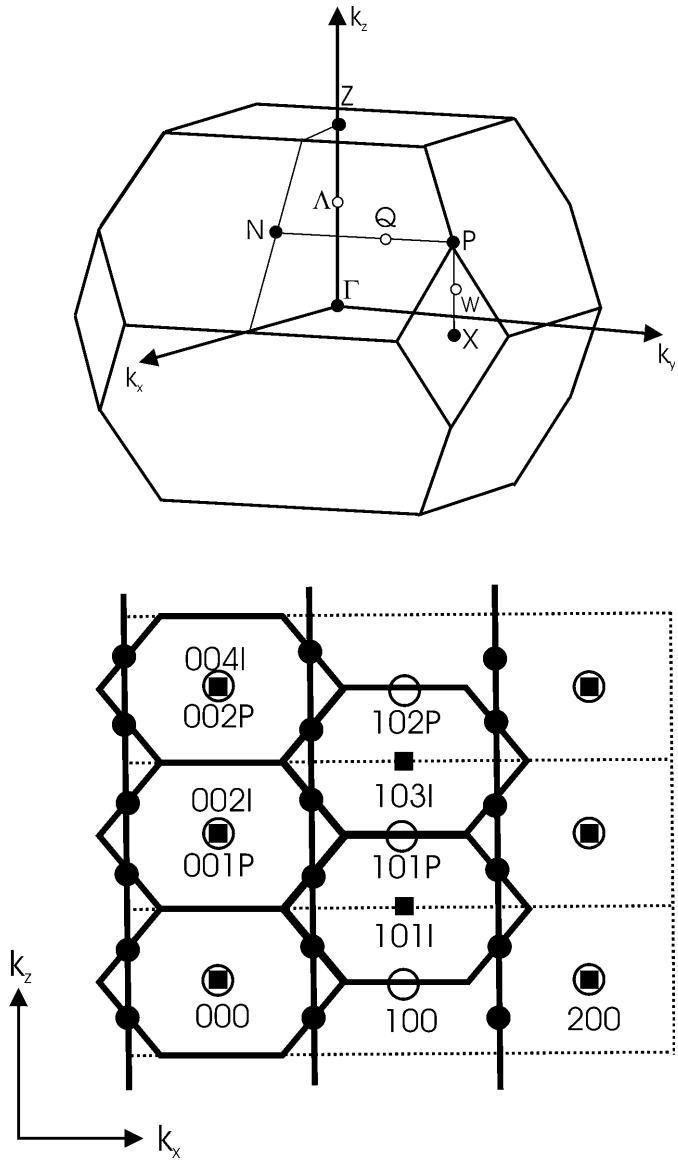

Figure 8
(*a*) The Brillouin Zone (BZ) of the I-centered layer perovskites. (*b*) Section of the BZs of the P-tetragonal ABX_4 and I-tetragonal A_2BX_4 perovskites. The layer spacing of A_2BX_4 is twice that of ABX_4 in this construction. Open circles represent the Γ-points of the P-tetragonal BZ. Closed squares represent the Γ-points of the I-tetragonal BZ. Hexagons represent the zone boundaries of the I-tetragonal BZ. Bold vertical lines represent the trace of the surface of pure tilts. Closed circles at the intersection of this trace with the I-tetragonal BZ boundary surface represent the *N*-points of this BZ. On the right hand side, the outline of the P-tetragonal BZ is shown in dotted lines.

Table 2
Labels, according to the convention of Miller & Love (1967), of the irreducible representations for the zero-frequency modes found for A_2BX_4 layer perovskites in the *Cmca* tilt system.

The left column shows the physical transformation of the irreducible representations at the Γ-point. A partial compatibility is given, only showing the zero-frequency modes at each point. The labels H_1 and H_3 are reversed with respect to the convention used by Muralt (1986). The Γ_2^+–Δ_4–Y_2^+ modes remain pure tilts.

T_x	Γ_3^-	Δ_4	Y_3^-			
T_y	Γ_4^-	Δ_1	Y_4^-	H_1	T_1	B_1 B_3
T_z	Γ_2^-	Δ_3	Y_2^-	H_3		
R_y	Γ_2^+	Δ_4	Y_2^+			
T_y	Γ_4^-	Σ_4	P_1	S_1		
T_z	Γ_2^-	Σ_3	P_2			
T_y	Γ_4^-	K_1	Λ_3	Z_1	B_1 B_3	
T_z	Γ_2^-	K_1	Λ_1			

The fact that incommensurates are seen for a wide variety of metals (Chapuis, 1978; Muralt, 1986; Doudin & Chapuis, 1988, 1992; Etxebarria *et al.*, 1988; Abid, 1994) indicates that the incommensurate transition is not driven by instabilities at the electronic Fermi surface. Also, the fact that they are not observed in either the analogues with simple cations or longer-chained cations implies that the packing of the relatively rigid PA chains drives the transition (Muralt, 1986; Kind & Muralt, 1986; Depmeier, 1981, 1983; Depmeier & Mason, 1978). So, to date, theoretical treatments of the incommensurate phases of PA salts have concentrated on these amines. Yet, the upper *I*4/*mmm*–*Cmca* α–β transition of PA_2MnCl_4 can clearly be related to a classical tilt transition in the A_2BX_4 structure (Hatch & Stokes, 1985, 1987, 1989). The same is true of the transition to the *Pbca* commensurately tilted, low-temperature phase of PA_2CdCl_4 (Chapuis, 1978; Doudin & Chapuis, 1988, 1992).

A calculation was performed for a layer, which had been subjected to a 5° [110] tilt with eigenvectors in the layer as shown in Fig. 6(*a*). There is a marked reduction in the number of zero-frequency modes. Instead of an instability at every **k**, there remain only two orthogonal planes of wavevectors containing zero-frequency modes, and special directions and points lying in these planes. These planes define wavevectors associated with all the possible incommensurate phases in these systems, if buckling modes of the layers are involved. Table 2 shows the corresponding symmetry labels for the A_2BX_4 layer perovskites, laid out in the form of a partial compatibility table, showing only those components with zero

frequency. The distribution of these modes in the ABX_4 and A_2BX_4 (tilt systems *Pmna* and *Cmca*, respectively) is shown in Fig. 9. For *Cmca*, the two planes *P* and *K*, in which the potential soft modes lie, generally have two distinct modes: there are two modes with K_1 symmetry, one mode with P_1 and one mode with P_2 symmetry. These modes become degenerate at certain zone-boundary positions, *e.g. S*, *Z*, *B* and *T*.

The phase transitions in these salts occur both due to the tilt instabilities in the layers and the ordering of the PA chains in PA_2MnCl_4. PA_2CuCl_4 shows an identical series of transitions (Etxebarria *et al.*, 1988). In the high-temperature α phase the amine groups sit in a site which is fourfold coordinated by apical halide atoms, with all four possible orientations equally occupied. Upon cooling the ordering of the cations begins and is correlated to the sequence of phase transitions observed; in the γ phase the cation is now partly ordered across the four sites. In the ζ phase all four sites become inequivalent and the PA chain becomes fully ordered (Kind & Muralt, 1986).

γ-PA_2MnCl_4 is characterized by transverse modulations running along **c** with amplitudes parallel to the *b* layer axis. The principal wavevector associated with this is $\mathbf{k} = (1/6 + \delta)\boldsymbol{c}^* + \boldsymbol{b}^*$ (Muralt, 1986; Kind & Muralt, 1986; Muralt *et al.*, 1988) and lies on the surface of the BZ along the isolated *H* line of the buckling modes (Fig. 9). Instead of a distinct lock-in transition, the order parameter, the amplitude of the incommensurate distortion, continuously decreases to zero. Thus, the *Cmca* β phase 'reappears' as the δ phase. The second incommensurate phase, ε, appears below this as a second-order transition with $\mathbf{k} = (1/3 + \delta)\boldsymbol{a}^*$ (Kind & Muralt, 1986). The wavevector for this mode is also shown in Fig. 9, lying along the Σ direction, a special direction lying in the P plane $\{\xi, \zeta, 0\}$.

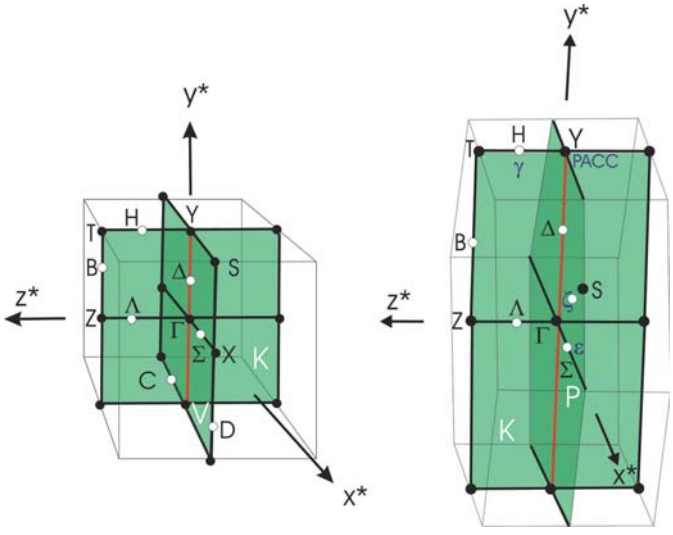

Figure 9
The distribution of RUMs through the Brillouin Zone (BZ) of commensurately tilted layers of ABX_4 and A_2BX_4 perovskites. The phases these correspond to are *Pmna* (left) and *Cmca* (right), respectively. A set of pure R_y tilts runs along Γ–Δ–*Y*. All other modes are buckling modes. Two general planes of modes lie in $\{\xi, \zeta, 0\}$ and $\{\xi, 0, \zeta\}$. In the BZ of *Cmca* the wavevectors of the γ, ε and ζ modulated phases of PA_2MnCl_4 are shown. The PACC symbol refers to the lowest-temperature phase of PA_2CdCl_4, which is commensurately tilted in the space group *Pbca* and is associated with ordering at the *Y*-zone boundary point. The wavevector associated with the ε phase of PA_2MnCl_4 also lies in the same direction as the single incommensurate phase reported for PA_2CdCl_4. The wavevector of the commensurately modulated ζ phase is free by symmetry to vary within the P plane.

Interestingly, the lock-in to the ζ phase occurs at yet another wavevector, $\mathbf{k} = (\boldsymbol{a}^* \pm \boldsymbol{b}^*)/3$, rather than at $1/3\boldsymbol{a}^*$ (Depmeier & Mason, 1978; Depmeier, 1981, 1983; Muralt, 1986; Kind & Muralt, 1986). Although it lies along the Γ–*S* line (Muralt *et al.*, 1988), this wavevector does not lie on a special line of symmetry, but generally in the P plane of zero-frequency buckling modes. Muralt *et al.* (1988) performed extensive symmetry analysis and noted that the irreducible representations responsible for the ε phase and the ζ phase are compatible. From this approach the physical reason for this compatibility is clear: the entire P plane is potentially soft and the Σ line of potential soft modes is a line of higher symmetry lying in this general plane.

The Weissenberg study of the γ phase by Depmeier (1981) reported satellites associated with the modulation occurring at A1 $(h, k, l \pm\delta_1)$, where $h + k = 2n + 1$, A2 $(h, k, l \pm 2\delta_1)$, where $h + k = 2n$, and B $(h, k, l \pm \delta_2)$, where $h + k = 2n + 1$. The A2 satellites are thought to be second-order reflections of the modulation or possibly second harmonics of the primary modulation (Muralt, 1986). While it could be that the B satellites are either pure artefacts, as suggested by Muralt (1986), or induced by stress on the sample, it is noticeable that they also lie along the *H* line of modes (Table 2; Fig. 9), and there is no limit to the number of modulations of octahedra in a sheet along this direction in *k*-space. It has been reported that weak satellites were also observed in *h*0*l* sections, implying that there was a longitudinal component to the mode, which had been previously presumed to be purely transverse (Depmeier, 1981). Table 1 shows that the BZ volume-filling buckling instabilities in the untilted system are all compatible at the Γ-point to the mode transforming as displacements along the layer axis. However, that is not the case for *Cmca*. The H_1 mode is ultimately compatible with T_y displacements normal to the layer and H_3 to T_z displacements. Following the change in the BZ after the commensurate tilt transition into *Cmca*, the H_3 mode is the buckling mode 'folded back' from the H_1 mode at the *T* zone boundary, where both modes are degenerate and of symmetry T_1. At general points along H, both H_1 and H_3 buckling modes have components of displacement (T_z, T_y) and rotation (R_x) of the octahedra and therefore both show transverse and longitudinal components with respect to the layers.

PA_2CdCl_4 also shows a transition from *Cmca* at room temperature to an incommensurate phase at 180 K with the wavevector $\mathbf{k} = 0.42a^*$, lying along Σ, as in the ε phase of PA_2MnCl_4, to *Pbca* at 158 K (Chapuis, 1978; Doudin & Chapuis, 1988, 1992). The refinements of this incommensurate phase also show rotations of fairly rigid octahedra coupled with modulated layer displacements. Unlike the Mn salt, the low-temperature ordered state is not a commensurately modulated phase but is associated with ordering associated with the Y_2^+ tilt mode of *Cmca* (Table 2; Fig. 9).

Early on in the investigation of these phases, the two-mode model of Heine & McConnell (1981) was suggested as a means of understanding the origin of the incommensuration, where it was suggested that the two modes were the rotation of the octahedra and the displacement of the layer (Doudin & Chapuis, 1988). This work has shown that tilting and layer modulation are component eigenvectors of a single phonon mode native to a layer perovskite (Table 1) and so can only form one mode in such a model. The later model of Doudin & Heine (1990) provided a microscopic view of packing of the PA chains, as the origin of the incommensuration. It is the interaction of the cation packing (the primary driving mode) with the buckling instabilities (the secondary lattice mode) that is the origin of the incommensurate structures in these layer perovskites.

5. Relationship of the ABX_4 layer perovskites to the ABX_3 true perovskites

The relationship between the BZs of the P-tetragonal ABX_4 and P-cubic ABX_3 perovskites is simple to visualize as the fusing of layers (Fig. 1). This is equivalent to adding more constraints; fewer degrees of freedom are expected for the octahedra, so the k-space distribution of zero-frequency modes is much more limited in this case (Dove *et al.*, 1991; Giddy *et al.*, 1993; Hammonds & Dove, 1994).

Tilt modes propagating along $\mathbf{k} = (\frac{1}{2}, \frac{1}{2}, \xi)$ tilt octahedra in the xy plane. This imposes no restrictions on the values of R_z of the octahedra in neighbouring layers fused along c, *i.e.* they retain zero frequency. This is one of the lines of M_3^+–T_4–R_4^+ pure tilts (Giddy *et al.*, 1993; Howard & Stokes, 1998). Note that the general characteristic of these modes is that the pseudovectors representing the directions of rotation of the octahedra are parallel to the M–T–R line (Fig. 10).

One can view the M_3^+–T_4–R_4^+ line of R_z tilts as being inherited from the isolated line of M_3^+–V_4–A_3^+ tilts of the ABX_4 perovskites (Fig. 2, Fig. 10). This leaves open the relationship of the other two lines of degenerate tilt modes in ABX_3 to those in ABX_4 (Fig. 2, Fig. 10): those tilts with eigenvectors R_x and wavevectors $(\xi, \frac{1}{2}, \frac{1}{2})$, and those with eigenvectors R_y with wavevectors $(\frac{1}{2}, \xi, \frac{1}{2})$. Consideration of the R_y tilt mode of a single layer with $\mathbf{k} = a^*/2$ in Fig. 3(*a*) shows that it would be impossible to fuse two layers together unless the waves were exactly out of phase in the ac plane, thereby requiring a component to the wavevector of $c^*/2$. This limits the dispersion of R_y tilts of rigid octahedra to the wavevectors $(\frac{1}{2}, \xi, \frac{1}{2})$. This corresponds to the R_3^+–T_2–A_5^+ line of modes in ABX_4 (Table 1, Fig. 2, Fig. 7), the only part of the F_2 plane of tilts that survives the constraint of fusion. Experimental evidence for the shallow dispersion of modes along the BZ edges has previously been obtained from inelastic neutron scattering (Shapiro *et al.*, 1974) and these lines have also been seen in computer simulations (Stixrude *et al.*, 1996).

5.1. Incommensurate organic–inorganic true perovskites

The best structurally determined, incommensurate, true perovskite appears to be $TMAGeCl_3$. The δ phase of $TMAGeCl_3$ has an incommensurate wavevector of $0.14\boldsymbol{b}^*$ when indexed in the *Pnam* orthorhombic phase (Fütterer *et al.*, 1995), equivalent to $0.14\boldsymbol{c}^*$ in *Pnma*, the setting used in the descriptions and analysis below. Fütterer *et al.* (1995) gave the following details: There is a transverse distortion with a maximum displacement along b, and the Ge and Cl displacements are close to being in-phase. Both $GeCl_3$ and TMA can be regarded as near rigid units and it seems very difficult to describe this transition in terms of the activity of a lone pair on Ge^{2+}. The motion appears to be consistent with layers of the two ions oriented perpendicular to a. The same bc shearing is involved between the orthorhombic and incommensurate phase as between the orthorhombic and the lock-in monoclinic phase.

This description is consistent with the distortion from a frozen transverse acoustic phonon, propagating along c^* with displacement eigenvectors along **b**. At $\mathbf{k} = 0.14\boldsymbol{c}^*$, relatively close to the Γ-point, both the TMA and $GeCl_6$ ions would still be nearly rigid bodies, the displacements along **b** and components in **a** being unaffected.

Table 3 shows the Γ-point irreducible representations and the basis functions that transform as pure translations along the cell axes, indicating the symmetries of the acoustic phonons. A compatibility table is given for acoustic phonons propagating along the cell directions. At $\mathbf{k} = 0.14\boldsymbol{c}^*$ the symmetry of this acoustic would be Λ_3. Therefore, the other

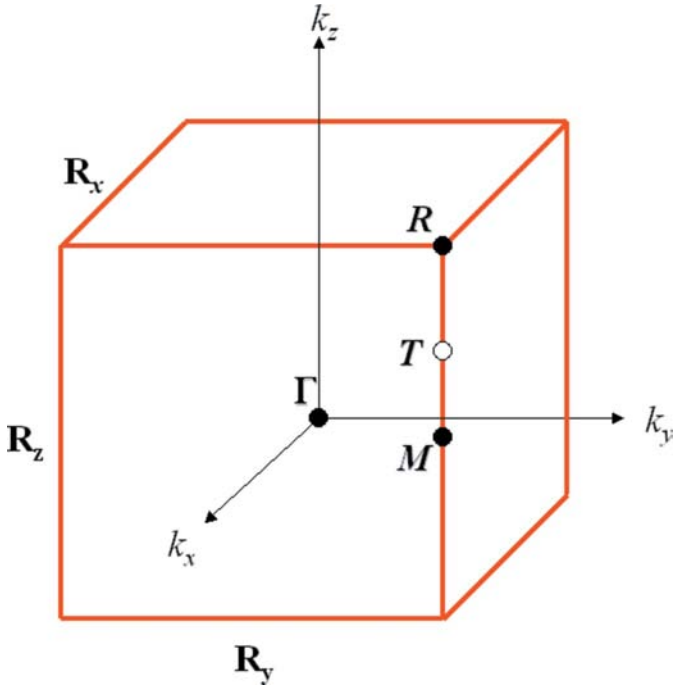

Figure 10
The Brillouin Zone (BZ) of the P-cubic true perovskites. Pure tilts are found along all the BZ edges (after Giddy *et al.*, 1993). The special points R and M and the line T are shown. The natures of the tilts are labelled along the edges: *e.g.* R_z propagating along $(\pm\frac{1}{2}, \pm\frac{1}{2}, \xi)$.

Table 3
Γ-point irreducible representations and their compatibility to the Λ-representations of *Pnma*.

The modes transforming as the basis functions T_x, T_y and T_z are given. For the acoustic phonons propagating along Λ (0,0,ξ), the symmetries of the longitudinal and two transverse acoustics are given. The basis function for the components of the polarizability tensor are also given from the tables of Fateley *et al.* (1972).

Γ	Γ	(00ζ)	Acoustic		Polarizability
Γ_1^+	A_g	Λ_1			α_{xx}, α_{yy}, α_{zz}
Γ_2^+	B_{1g}	Λ_2		R_z	α_{xy}
Γ_3^+	B_{3g}	Λ_3		R_x	α_{yz}
Γ_4^+	B_{2g}	Λ_4		R_y	α_{xz}
Γ_1^-	A_u	Λ_2			
Γ_2^-	B_{1u}	Λ_1	LA	T_z	
Γ_3^-	B_{3u}	Λ_4	TA_1	T_x	
Γ_4^-	B_{2u}	Λ_3	TA_2	T_y	

mode involved in incommensuration would be a low-frequency optic, presumably associated with the TMA cation ordering. This must transform as Λ_3 at $\mathbf{k} = 0.14\boldsymbol{c}^*$, but to something other than B_{2u} at the Γ-point, restricting the Γ-point symmetry of the low-lying optic to B_{3g}, which may be measurable by Raman spectroscopy as it transforms as α_{yz} (Table 3).

The incommensurate structure of $MAPbCl_3$ has not been determined but the positions of the incommensurate satellites do not lie along the *T* directions of the cubic precursor (Fig. 10). This cell appears to be quasi-tetragonal with incommensurate satellites approximately at $(\frac{1}{3},0,0)$ of the cubic lattice (Kawamura & Mashiyama, 1999). Pure tilt modes cannot be part of the incommensurate distortion. It seems likely that this would also involve an acoustic mode coupled to an ordering of the MA cation, in a manner similar to $TMAGeCl_3$. A full refinement of the incommensurate phase would be needed to confirm this.

6. Conclusions

A survey of the potential instabilities of untilted, isolated perovskite layers has been performed. There is a potential instability at all wavevectors in the aristotype structure. The nature of the eigenvectors of the zero-frequency modes vary continuously from pure tilts at $(\pm\frac{1}{2}, \xi, \zeta)$, $(\xi, \pm\frac{1}{2}, \zeta)$ to pure layer translations along the Γ–Λ–Z line, through modes of mixed buckling character at intermediate **k**. For A_2BX_4 perovskites in the *Cmca* tilt system, from which the modulated phases descend in the PA salts, the layer of octahedra becomes significantly more rigid, leaving only two residual planes of zero-frequency buckling modes (Fig. 9). The only pure tilts remaining lie along the Γ_2^+–Δ_4–Y_2^+ line of compatibility. All the modulated phases described to date for PA_2BX_4 show ordering vectors that lie on one of the solutions predicted by this approach. Despite the availability of pure tilts that could condense at incommensurate wavevectors, it does not appear that any such incommensurate structures have been reported for the organic inorganic perovskites. For the true perovskites, even in their highest symmetry, pure tilts are isolated in a single line in **k**-space and are not volumetrically important in the BZ.

When considered in isolation, the amines are effectively rigid molecular cations with six degrees of freedom and the only constraints that are imposed upon them are done so by interactions with the concatenated inorganic anion layer. The latter has a reduced degree of flexibility once tilted and it is this more constrained component that limits the flexibility of the entire system, by offering only a finite number of conformations. It is notable that the results from this approach are consistent with two of the more unusual features in the PA_2MnCl_4 system.

This approach is not, however, capable of predicting which of these possible wavevectors will actually cause a phase transition. For that a more holistic approach, taking into account the detailed interactions between both organic and inorganic components, is required; organic–inorganic perovskites display coupled tilt and orientational order–disorder transitions associated with the two components.

I would like to thank Drs Dorian Hatch, Harold Stokes (both of Brigham Young University), and Martin Dove and Andrew Goodwin (both of the University of Cambridge) for public provision of the codes ISOTROPY and CRUSH, without which this work would not have been possible.

References

Abid, Y. (1994). *J. Phys. Condens. Matter*, **6**, 6447–6454.
Aleksandrov, K. S., Beznosikov, B. V. & Misyul, S. V. (1987). *Phys. Status Solidi A*, **104**, 529–543.
Barman, S., Venkataraman, N. V., Vasudevan, S. & Seshadri, R. (2003). *J. Phys. Chem. B*, **107**, 1875–1883.
Bradley, C. J. & Cracknell, A. P. (1972). *The Mathematical Theory of Symmetry in Solids. Representation Theory for Point Groups and Space Groups.* Oxford: Clarendon Press.
Bulou, A., Launay, J. M., Rousseau, M., Ridou, C. & Nouet, J. (1984). *Ferroelectrics*, **54**, 249–252.
Bulou, A., Rousseau, M. & Nouet, J. (1987). *Phase Transit.* **9**, 139–145.
Bulou, A., Rousseau, M., Nouet, J., Loyzance, P. L., Mokhlisse, R. & Couzi, M. (1983). *J. Phys. C*, **16**, 4527–4537.
Chapuis, G. (1978). *Acta Cryst.* B**34**, 1506–1512.
Chi, L., Swainson, I. P., Cranswick, L. M. D., Her, J.-H. & Stephens, P. W. (2005). *J. Solid State Chem.* **178**, 1376–1385.
Deblieck, R. (1986). *Acta Cryst.* A**42**, 318–325.
Deblieck, R., Van Tendeloo, G., Van Landuyt, J. & Amelinckx, S. (1985). *Acta Cryst.* B**41**, 319–329.
Depmeier, W. (1981). *Acta Cryst.* B**37**, 330–339.
Depmeier, W. (1983). *Solid State Commun.* **45**, 1089–1092.
Depmeier, W. & Mason, S. A. (1978). *Acta Cryst.* B**34**, 920–922.
Doudin, B. & Chapuis, G. (1988). *Acta Cryst.* B**44**, 495–502.
Doudin, B. & Chapuis, G. (1992). *Acta Cryst.* C**48**, 1218–1220.
Doudin, B. & Heine, V. (1990). *J. Phys. Condens. Matter*, **2**, 3237–3246.
Dove, M. T., Giddy, A. P. & Heine, V. (1991). *Trans. Am. Cryst. Assoc.* **27**, 65–74.
Etxebarria, J., Ruiz-Larrea, I., Tello, M. J. & Lopez-Echarri, A. (1988). *J. Phys. C*, **21**, 1717–1725.

Fateley, W. G., Dollish, F. R., McDevitt, N. T. & Bentley, F. F. (1972). *Infrared and Raman Selection Rules for Molecular and Lattice Vibrations: The Correlation Method*. New York, London, Sydney, Toronto: Wiley Interscience, John Wiley and Sons.
Fütterer, K., Depmeier, W. & Petricek, V. (1995). *Acta Cryst.* B**51**, 768–779.
Giddy, A. P., Dove, M. T., Pawley, G. S. & Heine, V. (1993). *Acta Cryst.* A**49**, 697–703.
Glazer, A. M. (1972). *Acta Cryst.* B**28**, 3384–3392.
Glazer, A. M. (1975). *Acta Cryst.* A**31**, 756–762.
Hammonds, K. D., Bosenick, A., Dove, M. T. & Heine, V. (1998) *Am. Mineral.* **83**, 476–479.
Hammonds, K. D. & Dove, M. T. (1994). *Am. Mineral.* **79**, 1207–1209.
Hammonds, K. D., Heine, V. & Dove, M. T. (1998). *J. Phys. Chem. B*, **102**, 1759–1767.
Hatch, D. M. & Stokes, H. T. (1985). *Phys. Rev. B*, **31**, 2908–2912.
Hatch, D. M. & Stokes, H. T. (1987). *Phys. Rev. B*, **35**, 8509–8516.
Hatch, D. M. & Stokes, H. T. (1989). *Phys. Rev. B*, **39**, 9282–9288.
Heine, V. & McConnell, J. D. C. (1981). *Phys. Rev. Lett.* **46**, 1092–1095.
Howard, C. J. & Stokes, H. T. (1998). *Acta Cryst.* B**54**, 782–789.
Howard, C. J. & Stokes, H. T. (2002). *Acta Cryst.* B**58**, 565.
Hua, G. L. (1989). *J. Phys. Condens. Matter*, **1**, 9301–9312.
Hua, G. L. (1991). *J. Phys. Condens. Matter*, **3**, 1371–1388.
Kawamura, Y. & Mashiyama, H. (1999). *J. Korean Phys. Soc.* **35**, S1437–S1440.
Kind, R. & Muralt, P. (1986). *Incommensurate Phases in Dielectrics* Vol. 2, *Materials*, edited by R. Blinc & A. P. Levanyuk, pp. 301–318. Amsterdam: Elsevier Science Publishers BV.
Lee, Y., Mitzi, D. B., Barnes, P. W. & Vogt, T. (2003). *Phys. Rev. B*, **68**, 020103-1–020103-4.
Levanyuk, A. P. (1986). *Incommensurate Phases in Dielectrics*, Vol. 1, *Fundamentals*, edited by R. Blinc & A. P. Levanyuk, ch. 1. Amsterdam: Elsevier Science Publishers BV.
Maalej, A., Abid, Y., Kallel, A., Daoud, A., Lautié, A. & Romain, F. (1997). *Solidus Status Commun.* **103**, 279–284.
Maalej, A., Bahri, M., Abid, Y. & Jaïdane, N. (1999). *Can. J. Phys.* **77**, 717–722.
Miller, S. C. & Love, W. F. (1967). *Tables of Irreducible Representations of Space Groups and Co-Representations of Magnetic Groups.* Boulder, Colorado: Pruett Press.
Mitchell, R. H. (2002). *Perovskites: Modern and Ancient.* Thunder Bay, Ontario: Almaz Press.
Mitzi, D. B. (2001). *J. Chem. Soc. Dalton Trans.* pp. 1–12.
Mitzi, D. B. & Liang, K. (1997). *J. Solid State Chem.* **134**, 376–381.
Muralt, P. (1986). *J. Phys. C*, **19**, 1689–1704.
Muralt, P., Kind, R. & Bührer, W. (1988). *Phys. Rev. B*, **38**, 666–679.
Poglitsch, A. & Weber, D. (1987). *J. Chem. Phys.* **87**, 6373–6378.
Shapiro, S. M., Axe, J. D., Shirane, G. & Riste, T. (1974). *Anharmonic Lattices, Structural Transitions and Melting*, edited by T. Riste, NATO ASI Applied Sciences Vol. 1, pp. 135–140. Leiden: Noordhoff Publishing.
Stokes, H. T. & Hatch. D. M. (2002). *ISOTROPY*6.4.2. Physics Department, Brigham-Young University, UT; http://stokes.byu.edu/isotropy.html.
Stixrude, L., Cohen, R. E., Yu, R. & Krakauer, H. (1996). *ArXiv:physics*/9610023 v1.
Swainson, I. P. & Dove, M.T. (1993). *Phys. Rev. Lett.* **71**, 193–196.
Swainson, I. P., Hammond, R. P., Soullière, C., Knop, O. & Massa, W. (2003). *J. Solid State Chem.* **176**, 97–104.
Wolff, P. M. de, Janssen, T. & Janner, A. (1981). *Acta Cryst.* A**37**, 625–636.